LA-12413

UC-712 and UC-706
Issued: June 1993

Superlattice Electroabsorption Radiation Detector

B. J. Cooke

Los Alamos
NATIONAL LABORATORY
Los Alamos, New Mexico 87545

SUPERLATTICE ELECTROABSORPTION RADIATION DETECTOR

by
B. J. Cooke

ABSTRACT

This paper provides a preliminary investigation of a new class of superlattice electroabsorption radiation detectors that employ direct optical modulation for high-speed, two-dimensional (2-D), high-resolution imaging. Applications for the detector include nuclear radiation measurements,[1,2] tactical guidance and detection (laser radar), inertial fusion plasma studies, and satellite-based sensors. Initial calculations discussed in this paper indicate that a 1.5-μm (GaAlAs) multi-quantum-well (MQW) Fabry-Perot detector can respond directly to radiation of energies 1 eV to 10 KeV, and indirectly (with scattering targets) up through gamma, with 2-D sample rates on the order of 20 ps.

I. INTRODUCTION

The detector uses superlattice electroabsorption to directly modulate a laser probe with incident radiation. A superlattice is composed of thin (approximately 100 Å), alternating layers of semiconductor materials whose mismatched valence- and conduction-band energies form a multi-quantum-well (MQW) structure. Incident radiation interacts with the MQW structure and generates electron-hole (e-h) pairs (Figure 1A). Through electric field screening, the generated e-h pairs perturb the energy position[†] of the first exciton[††] absorption peak as indicated in Figure 1B. We can detect the shift in the absorption peak by probing the MQW with a weak laser probe and measuring the laser's change in amplitude. Two salient features of the detector are (1) the incident radiation directly modulates the laser probe, allowing for high-speed operation and (2) all information is optically formatted, providing a practical means for the high-speed parallel transmission of large amounts of data.

II. OVERVIEW OF SUPERLATTICE PROPERTIES

II.1 SUPERLATTICE QUANTUM-WELL PROPERTIES

Superlattices are layered semiconductor structures whose layer thicknesses can be controlled with atomic monolayer precision (Figure 2A). The layers can be made with matched lattices, mismatched lattices (strained-layer superlattices, Figure 2B), and doped layers (acceptor/donor sites).[3]

[†]Quantum-confined Stark shift.

[††]Excitons are coupled e-h pairs with energy states below the band gap of the host material.

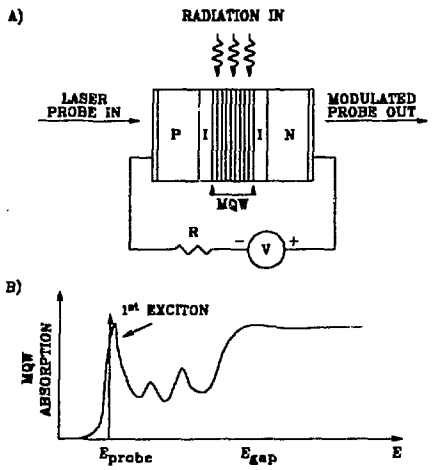

Figure 1. (A) Direct-conversion optical modulation (electroabsorption modulation). (B) Absorption spectrum of a MQW superlattice.

Of primary interest are the resulting quantum-well (QW) properties of very thin superlattice layers (approximately 100 Å). Within the superlattice layers, the motion of electrons and holes parallel to the layers is unrestricted. However, motion of the electrons and holes perpendicular to the layers is controlled by the discontinuities in potential at the layer interfaces. For very thin layers, the perpendicular motion of the electrons and holes is quantized. This quantization is due to the band structure encountered by the electrons and holes, which consists of a series of quantum wells (Figure 2C). One of the benefits of this quantization is the "freezing out" of one degree of freedom, resulting in a quasi-two-dimensional density of states (2D DOS). These

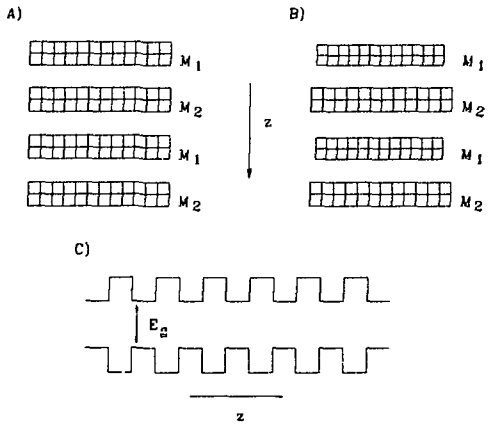

Figure 2. Superlattice structures. (A) Superlattice consisting of alternating layers M_1 and M_2. (B) Strained-layer superlattice. (C) Superlattice energy diagram.

superlattice quantum effects allow for the support of quantum-confined excitons, to be described next.

II.2 SUPERLATTICE QUANTUM-CONFINED EXCITONS

Excitons are bound e-h pairs whose quantized energy states lie below the band-gap edge. The physics of bulk semiconductor excitons are hydrogen-like (see Wannier excitons),[4] typified by spherical harmonic wave functions and energy solutions (Figure 3A). Bulk semiconductor excitons are observed at low temperatures through their optical absorption spectrum as shown in Figure 3B. Note the marked optical absorption below the band-gap energy at the exciton resonant energies. At higher temperatures (such as room temperature), the bulk excitons are ionized by phonon interactions and generally are not observable.

Superlattice quantum-confined excitons (Figure 3C, D) show a marked change in behavior when compared with their bulk counterparts.[5] Of primary note is the enhancement of exciton oscillator strengths and exciton stability at high temperatures (enhanced optical absorption of excitons at room temperatures). This enhancement can be directly attributed to the combination of two effects: (1) the quasi-2D density of states and (2) the quantum confinement of the exciton, resulting in distorted quasi-2D wave functions and hence, modified energy states (which are related to absorption energies and strengths).

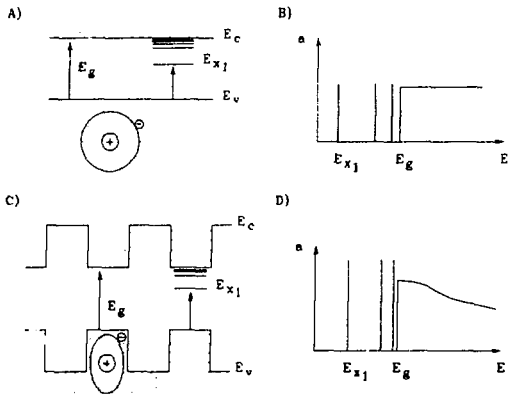

Figure 3. (A) Bulk exciton. (B) Absorption spectrum of bulk exciton. (C) Superlattice quantum-confined exciton. (D) Absorption spectrum of superlattice quantum-confined exciton.

III. EXCITON OPTICAL-ABSORPTION FIELD-DEPENDENCE (QUANTUM-CONFINED)

The exciton absorption spectrum undergoes a red shift (to longer wavelengths) when a field is applied as shown in Figure 4B. The optical-absorption field-dependence is the combined result of the quantum-confined Franz-Keldysh (QCFK) effect and quantum-confined Stark (QCS) effect.[6] A simplified QCFK and QCS explanation follows: The electric field distorts the exciton (Figure 4A), creating a small spatial separation (on average) between the electron-hole pairs. The spatial separation produces a reduction in the coulombic electron-hole pair binding energy, resulting in a red-shifted absorption spectrum. The quantum confinement prevents the electron-hole pairs from the premature ionization that would be expected in bulk material excitons. Note

that strained-layer superlattices generate strong internal fields, which in turn induce red-shifted absorption.[7]

Note that an internal or external field can be screened if there are enough free carriers present to retard or reverse red-shifted exciton absorption. The free carriers can be optically (radiation) induced or injected. Optically (radiation) induced free-carrier screening can lead to amplitude-dependent optical nonlinearities that will be exploited in the design of radiation detectors.

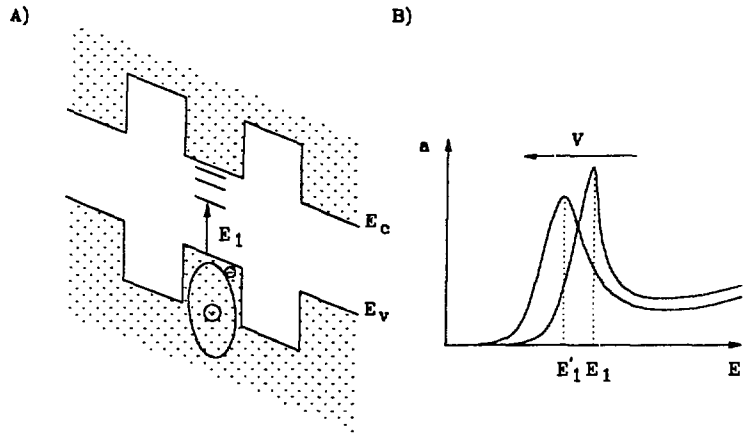

Figure 4. Exciton optical-absorption field-dependence. (A) Superlattice under external field. (B) Red-shifted exciton optical absorption.

IV. SUPERLATTICE NONLINEAR OPTICAL RESPONSE

The proper analysis of the optical nonlinearities in semiconductors requires the simultaneous solving of Maxwell's electromagnetic field equations and the nonlinear, time-dependent carrier density equations. The following derivation is adapted from Haug and Koch[8] except for the inclusion of the drift term in the continuity equation. Electromagnetic wave propagation in a dielectric medium is described by

$$[\nabla^2-\nabla(\nabla\cdot)-\frac{1}{c^2}\frac{\partial^2}{\partial t^2}]\mathbf{e}=\frac{4\pi}{c^2}\frac{\partial^2 \mathbf{P}}{\partial t^2},$$
$$\mathbf{P}=\chi\mathbf{e}, \qquad (1)$$
$$\chi=\chi_o+\chi_{nl}(N),$$

where $\mathbf{P}$ is the polarization and χ is the susceptibility of the semiconductor. Note that χ has been separated into its linear (χ_o) and density nonlinear ($\chi_{nl}(N)$) components. Assuming a z-propagating, Gaussian optical beam of the form

$$\mathcal{E}=\mathcal{E}_o\theta^{-(x^2+y^2)/w_o}, \tag{2}$$

where w_o is the characteristic transverse width of the beam, the incident electromagnetic wave can be separated into its longitudinal (e_z) and transverse (e_T) components with

$$\begin{aligned}
\nabla&=\theta_T\nabla_T+\theta_z\frac{\partial}{\partial t}\\
\mathcal{E}&=\theta^{-i(\omega t-kz)}(\theta_T e_T+\theta_z e_z)\\
P&=\theta^{-i(\omega t-kz)}(\theta_T P_T+\theta_z P_z),
\end{aligned} \tag{3}$$

resulting in (transverse)

$$\begin{aligned}
&\nabla_T[\nabla_T e_T+[ik+\frac{\partial}{\partial z}]e_z]-[-k^2+2ik\frac{\partial}{\partial z}+\frac{\partial^2}{\partial z^2}+\nabla_T^2]e_T\\
&=\frac{1}{c^2}[\omega^2+2i\omega\frac{\partial}{\partial t}-\frac{\partial^2}{\partial t^2}][e_T+4\pi P_T],
\end{aligned} \tag{4}$$

and (longitudinal)

$$[ik+\frac{\partial}{\partial z}]\nabla_T e_T-\nabla_T^2 e_z=\frac{1}{c^2}[\omega^2+2i\omega\frac{\partial}{\partial t}-\frac{\partial^2}{\partial t^2}][e_z+4\pi P_z]. \tag{5}$$

The following paraxial approximation assists in the decoupling of the transverse and longitudinal field components. If $f=1/kw_o << 1$, then scale x, y, z, and t by the Gaussian beam's characteristic width w_o,

$$\begin{aligned}
x&=\bar{x}w_o,\\
y&=\bar{y}w_o,\\
z&=\bar{z}w_o,\\
t&=\bar{t}(kw_o^2\frac{\sqrt{\epsilon_o}}{c}),\\
\omega&=\frac{\bar{\omega}}{\sqrt{\epsilon_o}},
\end{aligned} \tag{6}$$

and expand the transverse and longitudinal field components and the nonlinear susceptibility in powers of f:

$$e_T=e_T^{(0)}+f^2e_T^{(2)}+....$$

$$e_z=fe_z^{(1)}+f^3e_z^{(3)}+... \qquad (7)$$

$$\chi_{nl}=f^2\chi_{nl}^{(2)}+f^4\chi_{nl}^{(4)}+... \ .$$

Substituting into the wave equation and keeping components of order $O(f)$, the following holds true:

$$ke_z^{(1)}=i\nabla_T e_T^{(0)},$$

$$\left[\frac{c}{\sqrt{\epsilon_o}}\frac{\partial}{\partial z}-i\frac{c}{2k\sqrt{\epsilon_o}}\nabla_T^2+\frac{\partial}{\partial t}+\frac{c\alpha(\omega,N)}{2\sqrt{\epsilon_o}}-i\frac{\omega\Delta n(\omega,N)}{\sqrt{\epsilon_o}}\right]\epsilon_T^{(0)}=0, \qquad (8)$$

where

$$\alpha(\omega,N)=\frac{4\pi\omega}{\sqrt{\epsilon_o}c}\chi''(\omega,N),$$

$$\Delta n(\omega)\approx\frac{2\pi\chi_n'(\omega,N)}{\sqrt{\epsilon_o}} \qquad (9)$$

are the absorption- and refractive-index change, respectively. Finally, the field intensity and carrier density (N) are related through the continuity equation

$$\frac{\partial N}{\partial t}=-\frac{N}{\tau}+\frac{\alpha(\omega,N)}{\hbar\omega}I+\nabla D\nabla N+\nabla\mu NE,$$

$$I=\frac{|e|^2c\sqrt{\epsilon_o}}{8\pi}, \qquad (10)$$

where

τ = carrier relaxation time,
D = e-h diffusion coefficient,
μ = e-h mobility, and
E = static electric field.

V. FABRY-PEROT RESONATOR

A Fabry-Perot resonator structure is shown in Figure 5. The structure is composed of a dielectric medium of length l sandwiched between two partially reflective mirrors. The mirrors are

defined by their respective reflectivity (R) and transmissivity (T). For an incident field E_o, the resulting reflected component E_1 is given by

$$E_1 = T_1^2 R_2 E_o e^{-i2kl}[1 + R_1 R_2 e^{-i2kl} + R_1^2 R_2^2 e^{-i4kl} + \ldots]$$
$$= E_o[\frac{T_1^2 R_2 e^{-i2kl}}{1 - R_1 R_2 e^{-i2kl}}], \tag{11}$$

while the transmitted field is

$$E_2 = T_1 T_2 E_o e^{-ikl}[1 + R_1 R_2 e^{-i2kl} + R_1^2 R_2^2 e^{-i4kl} + \ldots]$$
$$= E_o[\frac{T_1 T_2 e^{-ikl}}{1 - R_1 R_2 e^{-i2kl}}], \tag{12}$$

where $ik = \alpha + i\beta$. Hence, the reflected and transmitted power are given by

$$|\frac{E_1}{E_o}|^2 = \frac{T_1^4 R_2^2 e^{-2\alpha l}}{(e^{\alpha l} - R_1 R_2 e^{-\alpha l})^2 + 4R_1 R_2 \sin^2(\beta l)},$$
$$|\frac{E_2}{E_o}|^2 = \frac{T_1^2 T_2^2}{(e^{\alpha l} - R_1 R_2 e^{-\alpha l})^2 + 4R_1 R_2 \sin^2(\beta l)}, \tag{13}$$

respectively.

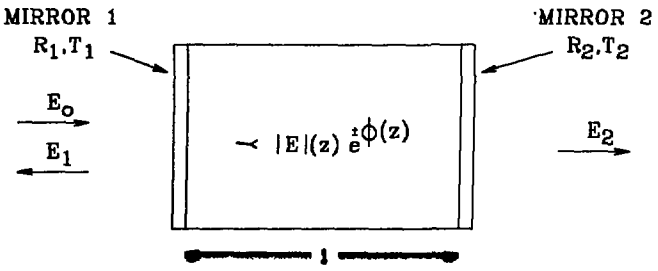

Figure 5. Fabry-Perot resonator.

VI. NONLINEAR ABSORPTION MODELS

Nonlinear absorption models are currently a hot research topic and can be readily found in the literature, depending on the application.[9,10,11,12]

VII. ELECTROABSORPTION PIN-DIODE MODULATOR

A P-doped/intrinsic/N-doped (PIN) diode electroabsorption modulator and the first exciton absorption spectrum are shown in Figures 6A and B, respectively. The PIN-diode configuration provides for voltage biasing and rapid removal of photogenerated electron-hole pairs. An example of operation follows: The voltage supply applies a reverse bias across the diode, creating a red shift in the first exciton absorption peak. External radiation (see Figure 1) generates electron-hole pairs that screen the applied electric field, causing a blue shift in the first exciton absorption peak. A shift in the exciton peak is detected by the corresponding change in the absorption characteristics of the laser probe. In Figure 6, the probe on the left provides a red-shift detection, while the probe on the right provides a blue-shift detection.

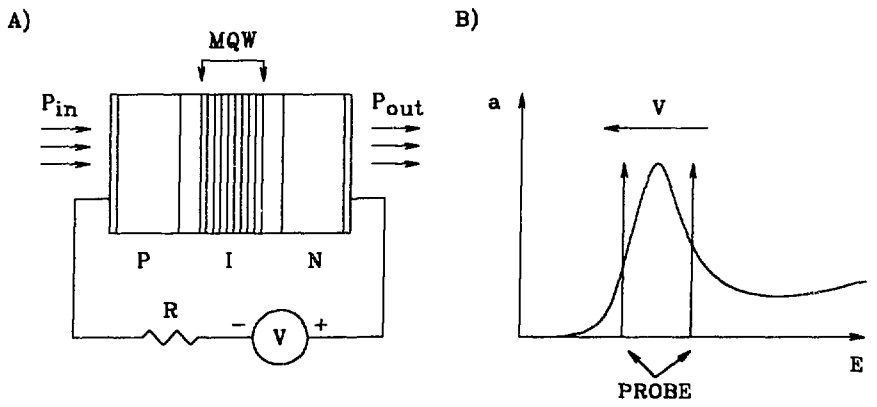

Figure 6. (A) Electroabsorption PIN-diode modulator. (B) First exciton absorption spectrum with probe energies superimposed.

VII.1 THIN-CAVITY FABRY-PEROT RESONATOR APPROXIMATION OF THE PIN-DIODE MQW

The optical response of the PIN-diode MQW cavity can be approximated with a thin-cavity Fabry-Perot resonator model. The electromagnetic field equations are derived as follows. Neglecting the transverse component, the wave equation (Equation 8) can be written in terms of magnitude and phase (Figure 5):

$$\left[\frac{\partial}{\partial z}+\frac{\sqrt{\epsilon_o}}{c}\frac{\partial}{\partial t}+\frac{\alpha(\omega,N)}{2}\right]|E|(z)=0,$$
$$\left[\frac{\partial}{\partial z}+\frac{\sqrt{\epsilon_o}}{c}\frac{\partial}{\partial t}\right]\phi(z)=\pm\frac{\omega\Delta n(\omega,N)}{c}. \tag{14}$$

For a thin sample (l small), the time variation of the magnitude and phase can be neglected (adiabatic approximation), hence,

$$\frac{\partial|E|(z)}{\partial t}\sim 0,$$
$$\frac{\partial\phi(z)}{\partial t}\sim 0, \tag{15}$$

resulting in

$$|E|(z)=E_o e^{-\frac{1}{2}\int_0^z \alpha(N(z'))dz'},$$
$$\phi(z)=\pm\frac{\omega}{c}\int_0^z \Delta n(N(z'))dz', \tag{16}$$

or,

$$\alpha=\int_0^l \alpha(N(z))dz,$$
$$\beta=-\beta_o-\frac{\omega}{c}\int_0^l \Delta n(N(z))dz. \tag{17}$$

Note that the intensity I, given in Equation 10, becomes

$$I=\frac{|\varepsilon|^2 c\sqrt{\epsilon_o}}{8\pi}\frac{1+\frac{R_1+R_2}{2}}{\frac{T_1+T_2}{2}} \tag{18}$$

for the Fabry-Perot resonator.

A calculation of the expected reflectivity as a function of the absorption coefficient for a 1.5-μm PIN-diode MQW Fabry-Perot resonator is shown in Figure 7. The calculation assumes the absorption coefficient is constant throughout the cavity and that the spatial carrier distribution $N(z)$ is spatially and temporally static.

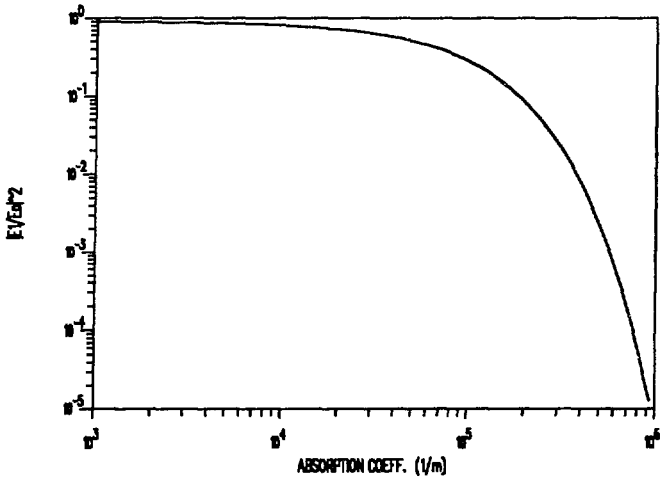

Figure 7. Reflectivity of a 1.5-μm PIN-diode MQW Fabry-Perot resonator for a 0.9-eV probe. $R1$ = 0.01, and $R2$ = 1.0.

VII.2 PIN-DIODE MQW CARRIER TRANSPORT

Solving for the characteristic response of the continuity equation (Equation 10) gives a preliminary evaluation of the PIN diode's temporal response in terms of its longitudinal drift and diffusion and transverse diffusion carrier transport. Rewriting Equation 10 in terms of the field-dependent diffusion and carrier drift velocity ($v_d=\mu E$) gives the following:

$$\frac{\partial N}{\partial t}=\frac{\alpha(\omega,N)I}{\hbar\omega}-\frac{N-N_o}{\tau}-v_i(E_i)\frac{\partial N}{\partial x_i}+D_{ij}(E_{ij})\frac{\partial^2 N}{\partial x_i \partial x_j}, \tag{19}$$

where $i,j = x,y,z$ and D_{ij} is the diffusion tensor. Note that a linear, isotropic medium with low carrier densities has been assumed. With the initial distribution $N(x,y,z,0)=A_o\delta(x)\delta(y)\delta(z)$, the characteristic solution with the electric field along the z-axis is

$$N(x,y,z,t)=\frac{A_o}{(4\pi t)^{\frac{3}{2}}\sqrt{D_{lo}}\sqrt{D_{tr}}\sqrt{D_{tr}}}\,e^{-\left[\frac{x^2+y^2}{4D_{tr}t}+\frac{(z-v_d t)^2}{4D_{lo}t}+\frac{t}{\tau}\right]}+N_o\,, \tag{20}$$

where D_{lo} and D_{tr} are the respective longitudinal and transverse components of the diffusion coefficients. The field-dependent velocity is given by the following expression:[13]

$$v_d(E)=\frac{\mu E+v_s(\frac{E}{E_o})^4}{1+(\frac{E}{E_o})^4}, \tag{21}$$

where typical values for the mobility, saturation velocity, and E_o are 8000 $cm^2/V\text{-}s$, 7.7×10^6 cm/s, and 4×10^3 V/cm respectively. Using the above values and neglecting diffusion, the carrier transit time across the MQW active region is 13 ps/μm or 19.5 ps for the 1.5-μm PIN-diode MQW Fabry-Perot device described above. Note that hot electron effects such as ballistic transport have not been included[14,15] (the effect of carrier ballistic transport is the reduction of device transit time). The total response time is given by

$$\frac{1}{\tau}=\frac{1}{\tau_{dr}}+\frac{1}{\tau_{dl}}+\frac{1}{\tau_r}, \tag{22}$$

where τ_{dr}, τ_{dl}, and τ_r are the respective drift, diffusion, and recombination time constants. Note that lateral diffusion with respect to drift must be minimized in order to maximize pixel resolution. This minimization should not be difficult if an electric field of any reasonable strength is present. A recent systematic study of carrier drift in quantum wells can be found in the literature.[16]

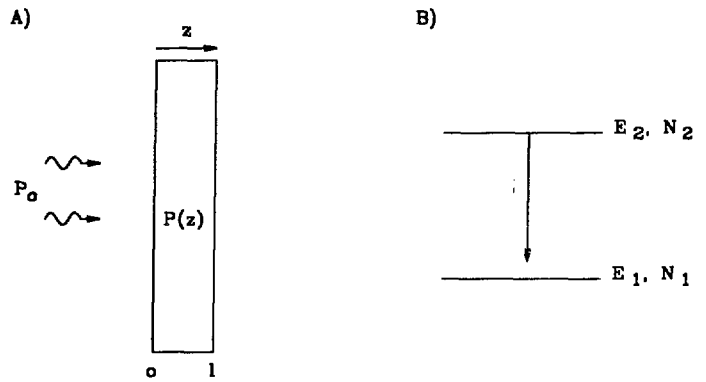

Figure 8. Atomic system absorption noise. (A) Material sample. (B) Schematic two-level system.

VII.3 PIN-DIODE MQW THERMAL EQUILIBRIUM NOISE LIMIT

The absorption noise for a system at thermal equilibrium can be approximated by a two-level system[17] (see Figure 8). The coherent attenuation of an optical beam with optical power $P(z)$ in a two-level absorbing system with energy and density N_1, E_1, and N_2, E_2, is given by

$$dP(z)=\alpha(\nu)P(z)dz \tag{23}$$

with

$$\alpha(\nu)=(N_2-N_1)\frac{c^2g(\nu)}{8\pi n^2\nu^2\tau}=N_1(e^{-\frac{h\nu}{kt}}-1)\frac{c^2g(\nu)}{8\pi n^2\nu^2\tau}, \tag{24}$$

where $g(\nu)$ is the spectral line shape function, τ is the spontaneous emission lifetime from E_2 to E_1, and n is the index of refraction. Solving for $P(z)$ given an incident power of P_o at the surface (z=0) in a sample with a given thickness l results in

$$P(z)=P_o e^{-\alpha(\nu)z}+\frac{h\nu\Delta\nu}{2e^{\frac{h\nu}{kT}}-1}(1-e^{-\alpha(\nu)z}). \tag{25}$$

For strong absorption ($e^{-\alpha l}$ << 1) and for $kT >> h\nu$,

$$P(l)=\frac{kT\Delta\nu}{2}, \tag{26}$$

indicating that the detector becomes Johnson-noise limited.

VII.4 PROTOTYPE PIN-DIODE MQW ELECTROABSORPTION DEVICE

A prototype electroabsorption detector is shown in Figure 9. A single-mirror PIN-diode MQW is shown in Figure 9A. The radiation enters through the front of the device, generates an electron-hole-pair density in the diode's active MQW region, and creates a red shift in the first exciton absorption spectrum. An optical probe then interrogates the surface of the device, and the output is reflected out to the probe detector. There are several important points to note: (1) The optical information is obtained in a parallel format (the entire detector surface is probed, and the information is extracted in a two-dimensional format as opposed to a serial format). (2) The probe's optical source can be remotely located and delivered through fiber-optic media, protecting the optical source. (3) The probe detector can be remotely located with the information piped out in a fiber-optic array bundle. The Fabry-Perot approximation of the PIN-diode MQW system is shown in Figure 9B. The two-mirror system forms the Fabry-Perot resonator discussed in Section VII.1, with the front mirror modeled as a low-reflectivity mirror.

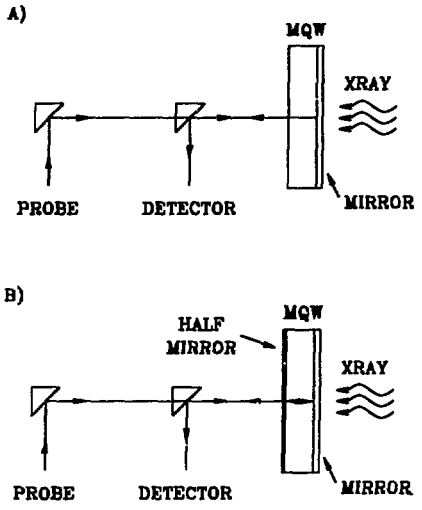

Figure 9. Prototype electroabsorption radiation detector. (A) Single-mirror detector. (B) Fabry-Perot model.

References

1. C. C. Cristopher, C. Eugster, and Peter L. Hagelstein, "X-Ray Detection Using Quantum Well Exciton Nonlinearity," *IEEE Journal of Quantum Electronics*, **26**(1), 75-84 (1990).

2. S. Basu, "Possibility of X-Ray Detection Using Quantum Wells," *IEEE Journal of Quantum Electronics*, **27**(9), 2116-2121 (1991).

3. C. Weisbuch, "Fundamental Properties of III-V Semiconductor Two-Dimensional Quantized Structures: The Basis for Optical and Electronic Device Applications," in *Semiconductors and Semimetals: Applications of Multiquantum Wells, Selective Doping, and Superlattices*, R. Dingle, Ed. (Academic Press Inc., San Diego, 1987), Vol. 24, pp. 1-29.

4. H. Haug and S. W. Koch, *Quantum Theory of the Optical and Electronic Properties of Semiconductors*, (World Scientific, New Jersey, 1990), pp. 148-175.

5. D. S. Chemla and D. A. B. Miller, "Nonlinear Optical Properties of Multiple Quantum Well Structures for Optical Signal Processing," in *Semiconductors and Semimetals: Applications of Multiquantum Wells, Selective Doping, and Superlattices*, R. Dingle, Ed. (Academic Press Inc., San Diego, 1987), Vol. 24, pp. 279-291.

6. D. A. B. Miller and D. S. Chemla, "Electric Field Dependence of Optical Properties of Semiconductor Quantum Wells: Physics and Applications," in *Optical Nonlinearities and Instabilities in Semiconductors*, Hartmut Haug, Ed. (Academic Press Inc., San Diego, 1988), pp. 325-359.

7. C. Mailhoit and D. L. Smith, "Effects of External Stress on the Structure and Optical Properties of [001]- and [111]- Growth-Axis Semiconductor Superlattices," *Physical Review B* **38**(8), 5520-5529 (1988).

8. H. Haug and S. W. Koch, *Quantum Theory of the Optical and Electronic Properties of Semiconductors*, (World Scientific, New Jersey, 1990), pp. 233-241.

9. D. S. Chemla, I. Bar-Joseph, J. M. Kuo, T. Y. Chang, C. Klingshirn, G. Livescu, and D. A. B. Miller, "Modulation of Absorption in Field-Effect Quantum Well Structures," *IEEE Journal of Quantum Electronics* **24**(8), 1664-1676 (1988).

10. G. Lengyel, K. W. Jelly, and R. W. H. Engelmann, "A Semi-Empirical Model for Electroabsorption in GaAs/AlGaAs Multiple Quantum Well Modulator Structures," *IEEE Journal of Quantum Electronics* **26**(2), 296-304 (1990).

11. H. Ando, H. Iwamura, H. Oohashi, and H. Kanbe, "Nonlinear Absorption in n-i-p-i MQW Structures," *IEEE Journal of Quantum Electronics* **25**(10), 2135-2141 (1989).

12. P. J. Stevens, M. Whitehead, G. Parry, and K. Woodbridge, "Computer Modeling of the Electric Field Dependent Absorption Spectrum of Multiple Quantum Well Material," *IEEE Journal of Quantum Electronics* **24**(10), 2007-2016 (1988).

13. S. Luryi, "Device Building Blocks," in *High Speed Semiconductor Devices*, S.M. Sze, Ed. (John Wiley & Sons, New York,1990), pp. 60-65.

14. E. Constant, "Non-Steady-State Carrier Transport in Semiconductors in Perspective with Submicrometer Devices," in *Topics in Applied Physics: Hot-Electron Transport in Semiconductors*, L. Reggiani, Ed. (Springer-Verlag, New York, 1985), Vol. 58, pp.227-261.

15. J. C. Bean, "Materials and Technologies for High-Speed Devices," in *High-Speed Semiconductor Devices*, S. M. Sze, Ed. (John Wiley & Sons, New York, 1990), pp. 14-20.

16. A. M. Fox, D. A. B. Miller, G. Livescu, J. E. Cunningham, W. Y. Jan, "Quantum Well Carrier Sweep Out: Relation to Electroabsorption and Exciton Saturation," *IEEE Journal of Quantum Electronics* **27**(10), 2281-2295 (1991).

17. A. Yariv, *Optical Electronics*, (Holt, Rinehart and Winston, Inc., New York, 1985).